

Physical Characterization of Cu₂basns₄ Thin Films Deposited At Different Concentrations of Sulfur Ions by Chemical Spray Pyrolysis Method

Hamsa J. Ata* , Nabeel A. Bakr , Asaad A. Kamil

Department of Physics, College of Science, University of Diyala

* hamsa93112@gmail.com

This article is open-access under the CC BY 4.0 license(http://creativecommons.org/licenses/by/4.0)

Received: 7 August 2024 Accepted: 9 September 2024

Published: October 2025

DOI: https://dx.doi.org/10.24237/ASJ.03.04.922C

Abstract

In this work, Cu_2BaSnS_4 thin films were deposited on soda-lime glass by the chemical spray pyrolysis technique (CSP) at different concentrations of thiourea, with a thickness of about 350 ± 10 nm measured by the gravimetric method. The thin films structural and morphological properties were investigated using X-ray diffraction (XRD), Raman spectroscopy, Field Emission Scanning Electron Microscopy (FE-SEM), and Atomic Force Microscopy (AFM), as well as optical properties using a UV-Vis spectrophotometer at the wavelength range (300–900) nm. We investigated the electrical properties using the Hall Effect. The optical band gap of CBTS thin films increased from (1.757 to 1.923) eV when concentrations of thiourea increased from (0.04 to 0.12) M. The Cu_2BaSnS_4 (CBTS) films have a high absorption coefficient ($\alpha > 10^4$ cm⁻¹), indicating allowed direct electron transmission. XRD measurements of Cu_2BaSnS_4 (CBTS) films revealed a trigonal crystal structure. The XRD pattern preferred the (104) orientation, which has a high intensity and indicates that crystallization is most likely to occur along this plan. Raman spectroscopy of CBTS thin films revealed a protruding peak at ~341 cm⁻¹. The morphological findings and FE-SEM photographs of the thin film surface revealed a variety of structures and forms, one of which resembled cauliflower. Electrical tests



revealed the conductivity of (p-type). The calculated electrical conductivity of CBTS thin films was found in the range of $0.053 - 0.184 \, (\Omega.\text{cm})^{-1}$. Based on our findings, the Cu₂BaSnS₄ (CBTS) thin films look to be an excellent choice for an absorber layer in solar cells.

Keywords: Cu₂BaSnS₄, chemical Spray pyrolysis, thin films, structural properties, optical properties

Introduction

The availability of solar energy at no cost has led to its recognition as a credible alternative source of energy [1,2]. Over the past few years, there has been a substantial increase in the quality of research on thin film-based solar cells. CuO, SnS, Cu₂SnS₃, Cu₂ZnSnS₄, CdTe, and Cu₂InGaS₂ are inorganic compounds that have garnered significant attention as light absorber materials in photovoltaic solar energy [3–8]. Cu₂ZnSnS₄ (CZTS) remains the most effective alternative to CdTe and Cu₂InGaS₂-based solar cells, with a power conversion efficiency of 12.6%, surpassing SnS, Cu₂SnS₃, and CuO [9]. Furthermore, CZTS possesses suitable characteristics, including a band gap that is nearly 1.5 eV, a high optical absorption coefficient exceeding 10⁴ cm⁻¹, and p-type electrical conductivity [10]. For these reasons, research groups considered enhancing certain quaternary materials that are derived from CZTS thin films by substituting certain chemical elements with those from the periodic table that are also low-cost and non-toxic in tetragonal, cubic, and trigonal structures. These materials are a potential alternative to CZTS and possess suitable properties for photovoltaic applications. Ag₂ZnSnS₄ is produced by substituting copper (Cu) with silver (Ag) to produce the derived absorber materials [11]. Additionally, the substitution of tin (Sn) with germanium (Ge) results in the formation of Cu₂ZnGeS₄ [12]. The exchange of zinc (Zn) with cobalt (Co) [13], nickel (Ni) [14], iron (Fe) [15], cadmium (Cd) [16], and barium (Ba) [17] results in the production of Cu₂CoSnS₄, Cu₂NiSnS₄, Cu₂FeSnS₄, Cu₂CdSnS₄, and Cu₂BaSnS₄, respectively. Copper barium tin sulfur (CBTS) is the most viable alternative to CZTS among these materials, as it inhibits the formation of antisite defects and exhibits associated band tailing with a band gap ranging from 1.3 to 2.01 eV. It is the primary alternative to CZTS due to its high optical absorption coefficients of up to 10⁴ cm⁻¹ and p-type semiconductor conductivity [18]. Additionally, the scientific researchers were motivated to develop a CBTS solar cell by the significant ionic size



mismatch between Ba²⁺ (1.49 A°) and Sn⁴⁺ (0.83 A°) and Cu⁺ (0.91 A°) [18]. The purpose of investigating CBTS thin films is to enhance certain physical characteristics of this material in anticipation of its potential application in photovoltaic solar cells. Various vacuum and non-vacuum methods, including co-sputtering [17], silar [19], sol–gel [20], and spray pyrolysis [21], can be employed to produce CBTS.

The (CBTS) thin film was synthesized at room temperature utilizing the chemical spray pyrolysis CSP technique, as shown in this study. Despite the lack of extensive study, the CSP technique is an environmentally friendly, cost-effective, and adaptable technology with high throughput and material utilization [22]. We looked at the thin films' structural, morphological, optical, and electrical characteristics. The CBTS thin films generated via spray pyrolysis also have semiconducting properties, making them a potential material for solar absorber synthesis.

Experimental Procedure

To investigate the properties of Cu₂BaSnS₄ thin films, the solution employed the materials enumerated in Table (1). The aqueous solution of copper nitrate Cu (NO₃)₂.3H₂O, barium nitrate Ba (NO₃)₂, stannic (Tin) chloride SnCl₄.5H₂O, and thiourea CH₄N₂S is sprayed to manufacture the Cu₂BaSnS₄ thin films. While maintaining the other parameters constant, CBTS thin films are produced at varying concentrations of Thiourea. The precursor solution is produced by adding aqueous solutions of 0.02 mol/L of Cu (NO₃)₂.3H₂O, 0.01 mol/L of Ba (NO₃)₂, 0.01 mol/L of SnCl₄.5H₂O, and (0.04, 0.06, 0.08, 0.1, and 0.12) mol/L of CH₄N₂S to a final volume of 100 mL. This solution is formed by dissolving the appropriate quantities of copper nitrate Cu (NO₃)₂.3H₂O, barium nitrate Ba (NO₃)₂, stannic (Tin) chloride SnCl₄.5H₂O, and thiourea CH₄N₂S in distilled water. Figure (1) shows the CSP technique schematically represents the film growing process.

Table 1: The raw materials used in the current study and their characteristics.



Properties	Cu (NO ₃) ₂ .3H ₂ O	Ba(NO ₃) ₂	SnCl ₄ . 5H ₂ O	CH ₄ N ₂ S
Density (g/cm ³)	2.32	3.24	3.9	1.4
Appearance	Blue	White	White	White
Solubility in Water	0.267g/0.1mL (20°C)	10.3g/0.1mL (25°C)	very soluble	14.2g/0.1mL (25°C)
Molecular Weight (g/mol)	241.6	261.34	350.58	76.11

The materials' appropriate weight (W_t) [Cu $(NO_3)_2.3H_2O$, Ba $(NO_3)_2$, SnCl₄. $5H_2O$ and CH₄N₂S] is found using the following equation:

$$\mathbf{M} = (\mathbf{W}_{t} / \mathbf{M}_{\mathbf{W}_{t}}). (1000/\mathbf{V}) \tag{1}$$

Where: -

M: is the specific molar concentration (mol/L).

 W_t : is the weight required to be dissolved (g).

 M_{Wt} : the molecular weight of the solute (g/ mol).

V: the volume of dissolved solvent (ml).

The weights of [Cu (NO₃)₂.3H₂O, Ba (NO₃)₂, SnCl₄.5H₂O and CH₄N₂S] are determined using a sensitive electronic balance (Mettler, AE -160) with a sensitivity of four digits (10⁻⁴g). The solutions are mixed using a magnetic stirrer and the solution is allowed to sit for one hour to ensure that no residues remain and that the resultant solution is homogeneous. The CBTS thin films are prepared by spraying the resultant solution onto preheated glass substrates at varying substrate thiourea concentrations. The concentrations and masses utilized in the preparation of the solution are illustrated in Table (2).

Table 2: Concentrations and masses used in preparing the solution.

Salt	Concentration (M)	Weight (g)	Volume of
			Distilled Water (mL)
Cu (NO ₃) ₂ .3H ₂ O	0.02	0.1208	25
Ba(NO ₃) ₂	0.01	0.0653	25
SnCl _{4.} 5H ₂ O	0.01	0.0876	25
CH_4N_2S	(0.04, 0.06, 0.08, 0.1	(0.0761, 0.1141, 0.1523,	25
	and 0.12)	0.1902 and 0.2283)	

The mechanism of the reaction is illustrated by the following equations.

$SnCl_4 + 5H_2O \longrightarrow Sn[(H_2O)_5]^{+4} + 4Cl^{-1}$	



$Ba(NO_3)_2 + 5H_2O \longrightarrow Ba[(H_2O)_5]^{+2} + 2NO_3$				
$NH_2CH_4N_2S + 2H_2O \longrightarrow 2NH_3 + H_2S + CO_2$				
$Cu(NO_3)_2 + 5H_2O \longrightarrow Cu[(H_2O)_5]^{+2} + 2NO_3^{-1}$				
$Sn[(H_2O)_5]^{+4} + 5NH_3$ $Sn[(NH_3)_5]^{+4} + 5H_2O$				
Ba[$(H_2O)_5$] ⁺² + 5NH ₃ Ba[$(NH_3)_5$] ⁺² + 5H ₂ O				
$Cu[(H_2O)_6]^{+2} + 5NH_3 \longrightarrow Cu[(NH_3)_5]^{+2} + 5H_2O$				
$H_2S \longrightarrow H^+ + SH^{-1}$				
$SH^{-1} \longrightarrow H^+ + S^{-2}$				
$Cu[(NH_3)_5]^{+2} + S^{-2}$ $CuS + 5NH_3$				
$Sn[(NH_3)_5]^{+4} + S^{-2}$ $SnS + 5NH_3$				
Ba[$(NH_3)_5$] ⁺² + S ⁻² BaS + 5NH ₃				
2CuS + SnS + BaS Cu ₂ BaSnS ₄				

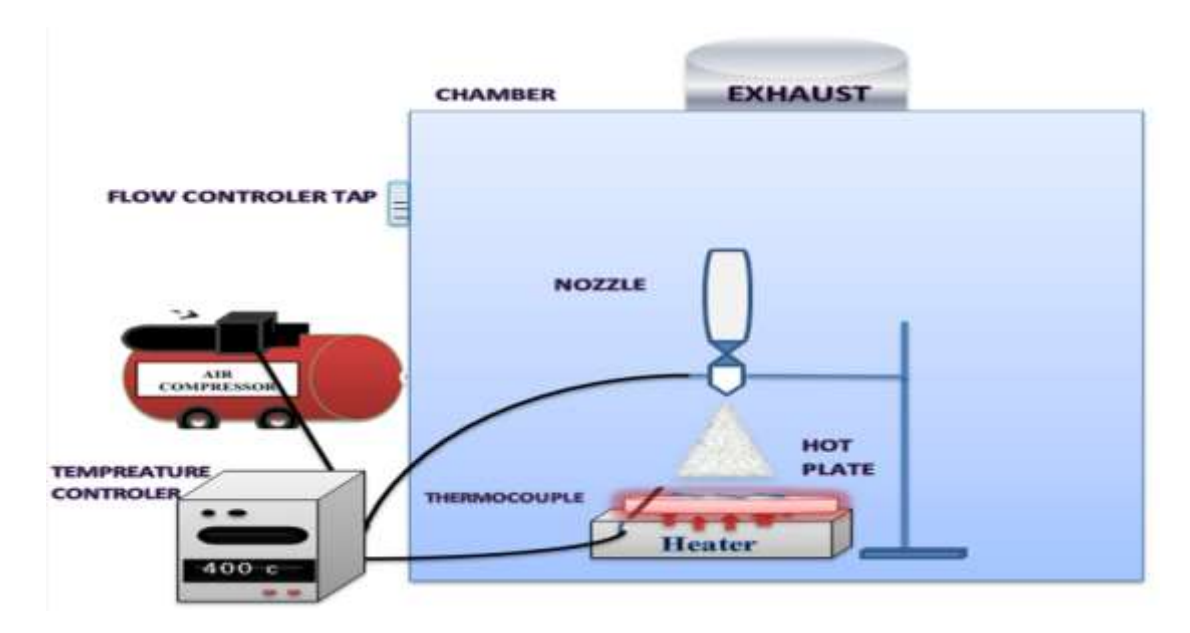


Figure 1: Illustration of the CSP process for creating CBTS thin films [5].

Characterization Techniques

The Bruker D8 Advance, a German instrument, captured the X-ray diffraction (XRD) patterns of the CBTS films. In this experiment, the Raman spectra were acquired using a He-Ne laser manufactured by Horiba Jobin-Yvon LabRam HR800. This device is comprised of a laser

source, a laser filter, and a detector, as well as a computer. It has an analysis capability of 1cm⁻¹ and operates at a wavelength of (632.81nm) to diagnose Cu₂BaSnS₄ thin films that have been prepared. The CBTS morphologies were analyzed using high-resolution atomic force microscopy (SPM-AA3000, Japan) and field emission scanning electron microscopy (FESEM, MIRA3 TESCAN, Czech). The UV-Vis spectroscopy technique (Shimadzu UV-1800, Japan) was used to examine the optical characteristics of the CBTS thin film. The Raman spectra were obtained using the HMS-3000 ECOPIA instrument from the United States of America.

Results and Discussion

Structural characteristics

Figure (2) illustrates the X-ray diffraction (XRD) patterns of Cu₂BaSnS₄ thin films deposited using the CSP technique. The pattern contains diffraction peaks at approximately (2θ: ~19°, 27°, 39°, 49°, 52°). The peak positions represent the (102), (104), (204), (108), and (215) planes, and these results are in agreement with the ICCD card (PDF 30-0124). The XRD patterns exhibited a strong preference for the (104) orientation, which is characterized by a high intensity. This suggests that crystallization is more likely to occur along this plane, as seen in Figure 2 [23].

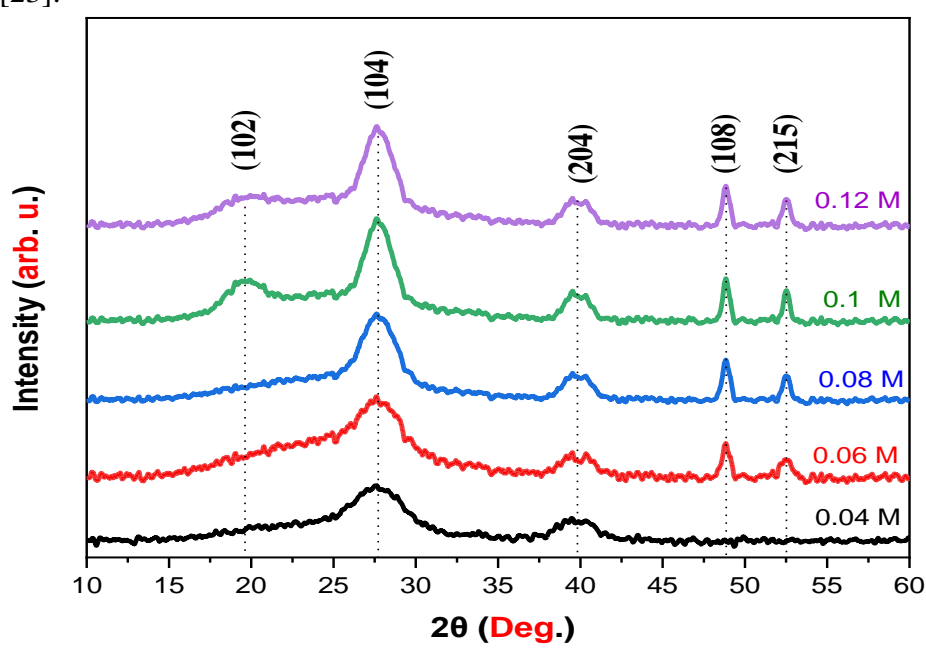


Figure 2: X-ray Diffraction of CBTS thin films deposited at different thiourea concentrations.



The strongest peak is located at $2\theta \sim 27^{\circ}$ [20, 24]. The lattice parameters of the prepared thin films were polycrystalline and trigonal crystal structures [20, 21]. The diffraction angle (2 θ), interplanar distance (d), full width at half maximum (FWHM), and phases identified on the (hkl) planes were all structural parameters examined utilizing these patterns. The corresponding values are listed in table (3). Crystal flaws induce stresses in the crystal lattice. Result in a very modest deviation in peak positions with a change in the thiourea concentration. With the increase in thiourea concentration, the peak intensity increases until it reaches its maximal value at 0.1 M. This concentration is characterized by a narrowing of the peaks, which suggests enhanced crystallization. Consequently, this concentration is the most suitable for the deposition of CBTS thin films. We observe that the peak (102) vanishes at concentrations of (0.04, 0.06, and 0.08 M). The Scherrer's formula was employed to determine the crystallite size of the Cu₂BaSnS₄ thin films for the (104) direction:

$$D = \frac{0.9 \,\lambda}{\beta \cos \theta} \tag{2}$$

Table 3: Structural parameters for (104) direction for CBTS thin films at different thiourea concentrations.

Thiourea Concentration (M)	0.04	0.06	0.08	0.1	0.12
full width at half maximum (FWHM) (rad)	0.056	0.046	0.04	0.042	0.046
Crystallite size (D) (nm)	2.527	3.083	3.55	3.352	3.072
Texture coefficient (Tc)	0.442	0.359	0.377	0.386	0.377
Number of Crystallites Per Unit Area (N ₀)×10 ¹⁴ (cm) ⁻²	21.686	11.936	7.821	9.292	12.062
Dislocation density (δ)×10 ¹² (cm) ⁻²	15.658	10.516	7.934	8.899	10.59

Where D is the crystallite size, λ is the wavelength of incident X-ray radiation = 1.5406Å for CuK_{α} , β is the (FWHM) of the peak (in radians), θ is the Bragg diffraction angle of the XRD peak. The dislocation density (δ) and number of crystallites per unit area can be determined using the following formulas:

$$\delta = 1/\mathbf{D}^2 \tag{3}$$

$$N_0 = t/D^3 \tag{4}$$



Where t is the thickness of the thin film. The crystallite size values in the (104) direction of CBTS thin films increase as the concentration of thiourea increases until it reaches a concentration of (0.1) M, then it starts decreasing as illustrated in table 3. The square of the crystallite size is inversely proportional to the density of dislocations [9].

Figure (3) illustrates the Raman spectra for CBTS thin films. The Raman spectra of all samples of the films in CSP method exhibit a distinct broad and wide peak at approximately (341 cm⁻¹) [19,23].

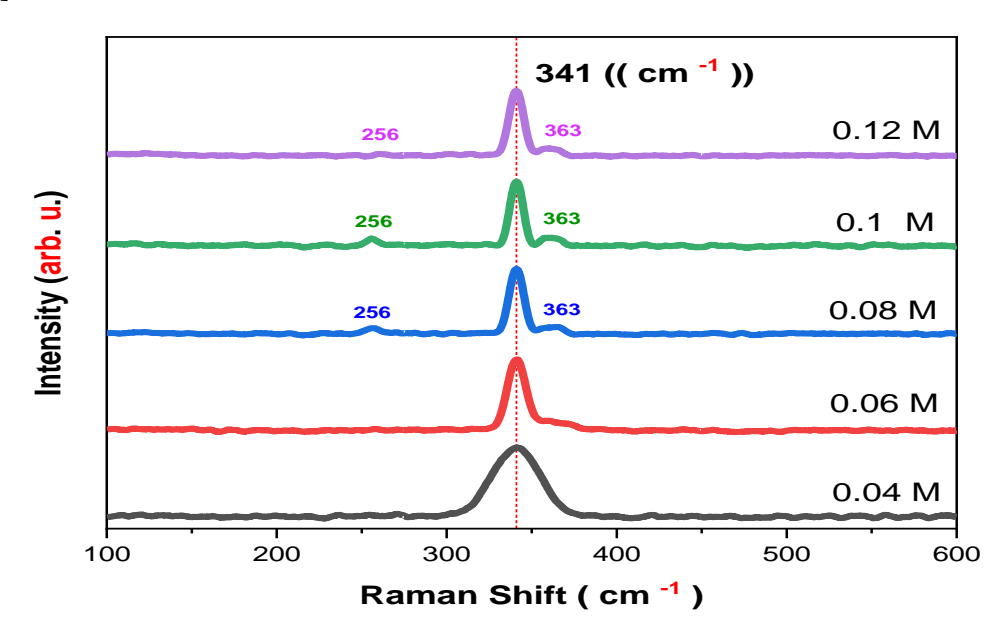


Figure 3: Raman Spectra for CBTS thin films at different thiourea concentrations.

These peaks are associated with trigonal CBTS, which are classified as symmetric vibrations in which the motion of sulphur atoms is subject to "A" symmetries [18,20]. Thin films produced very small peaks with lower intensity at (256 and 363 cm ⁻¹). The sample generated with a concentration of thiourea at a concentration of (0.1) M had the greatest intensity and the smallest width at half intensity as illustrated in Table (4). According to the findings of the X-ray diffraction analysis, the sample also had the highest degree of crystallinity. The samples demonstrate the most optimal crystallization at a concentration of 0.1 M thiourea, as indicated by the X-ray diffraction results. These findings are consistent with the X-ray diffraction results.



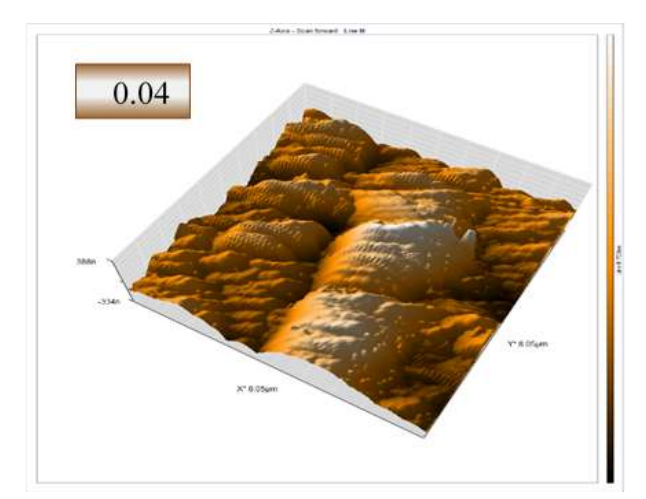
Table 4: Raman Spectra results of CBTS thin films prepared by CSP technique.

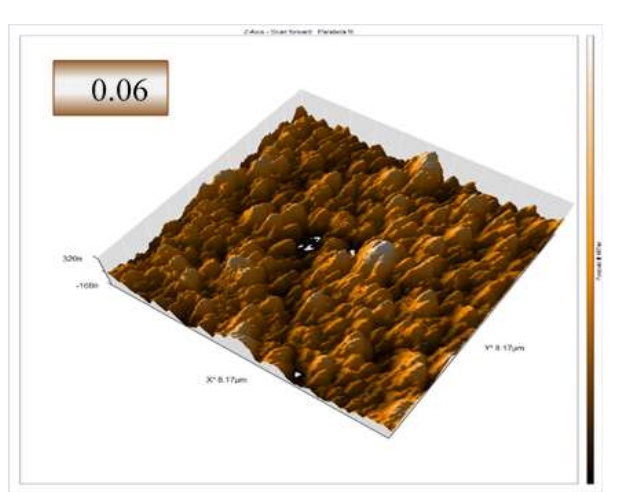
Thiourea Concentrations	Peak center	Peak width	Intensity
(M)	(cm ⁻¹)	(cm ⁻¹)	(arb. u.)
0.04	340.72	32.853	81.45433
0.06	340.51	14.862	88.89694
0.08	341.07	11.652	80.51439
0.1	341.24	10.134	88.95378
0.12	340.06	11.641	84.57547

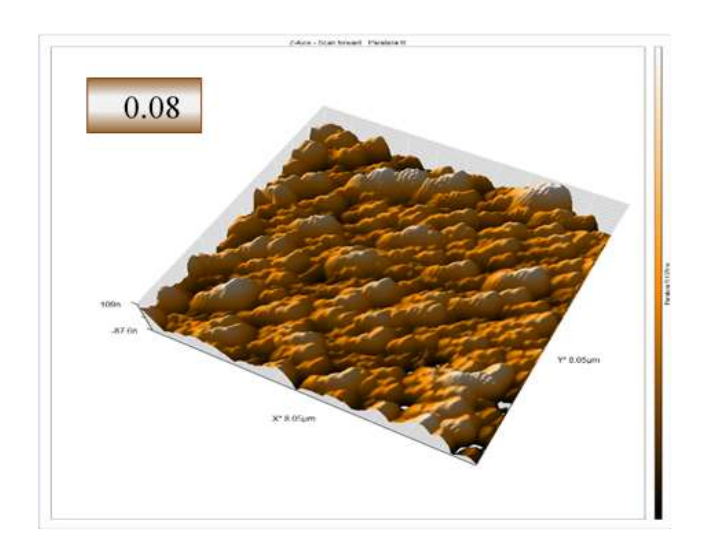
Morphological properties

The surface morphology of CBTS thin films with various concentrations of thiourea is analyzed using AFM, which yields the surface grain sizes directly. Figure (4 and 5) illustrate 3-D AFM images and the granularity accumulation distribution charts for CBTS thin films at varying thiourea concentrations, demonstrate a uniform island-like topography on the surface [17]. In the concentrated sample, the films maximal value for both surface roughness and root mean square are (0.04 M). It is evident from this table that the particle size fluctuates randomly from one zone to another, spanning a range of (68.93 and 278.7) nm. The FE-SEM device technology was employed to examine the microstructure features and surface morphology of the deposited thin films. It possesses an exceptional capacity to precisely photograph and magnify the surfaces of materials. At magnifications of 50 and 100 kx, Figure (6) displays images of Cu₂BaSnS₄ films at various concentrations of thiourea. FE-SEM images of samples were analyzed using Image J software to determine the influence of increasing sulfur concentration on the structure of prepared films, calculate the average particle size, and investigate the surface of thin films. Thin film surface structure of Cu₂BaSnS₄ thin films that have been prepared made up of cauliflower-like shapes. We can clearly see that thin films exhibit pinholes and voids in the images. Pinholes/cracks are frequently observed in thin films based on Cu chalcogenide as a result of particle growth or decomposition [25]. This material is composed of particles of different sizes, with a variety of surface shapes and an irregular distribution. Its growth is influenced by the presence of crystalline defects, which result in cracks and voids. Additionally, the presence of secondary growth on the surface suggests the formation of a new layer above the preceding one, and distinct grain boundaries are visible [26].









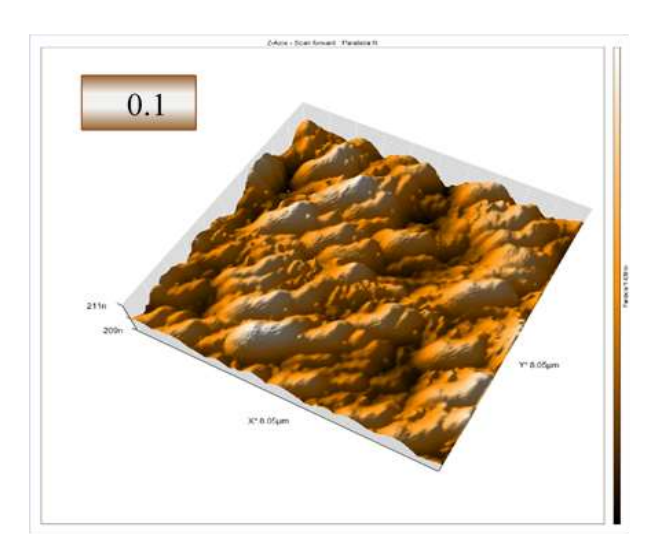




Figure 4: 3-D AFM images for CBTS thin films at different thiourea concentrations.



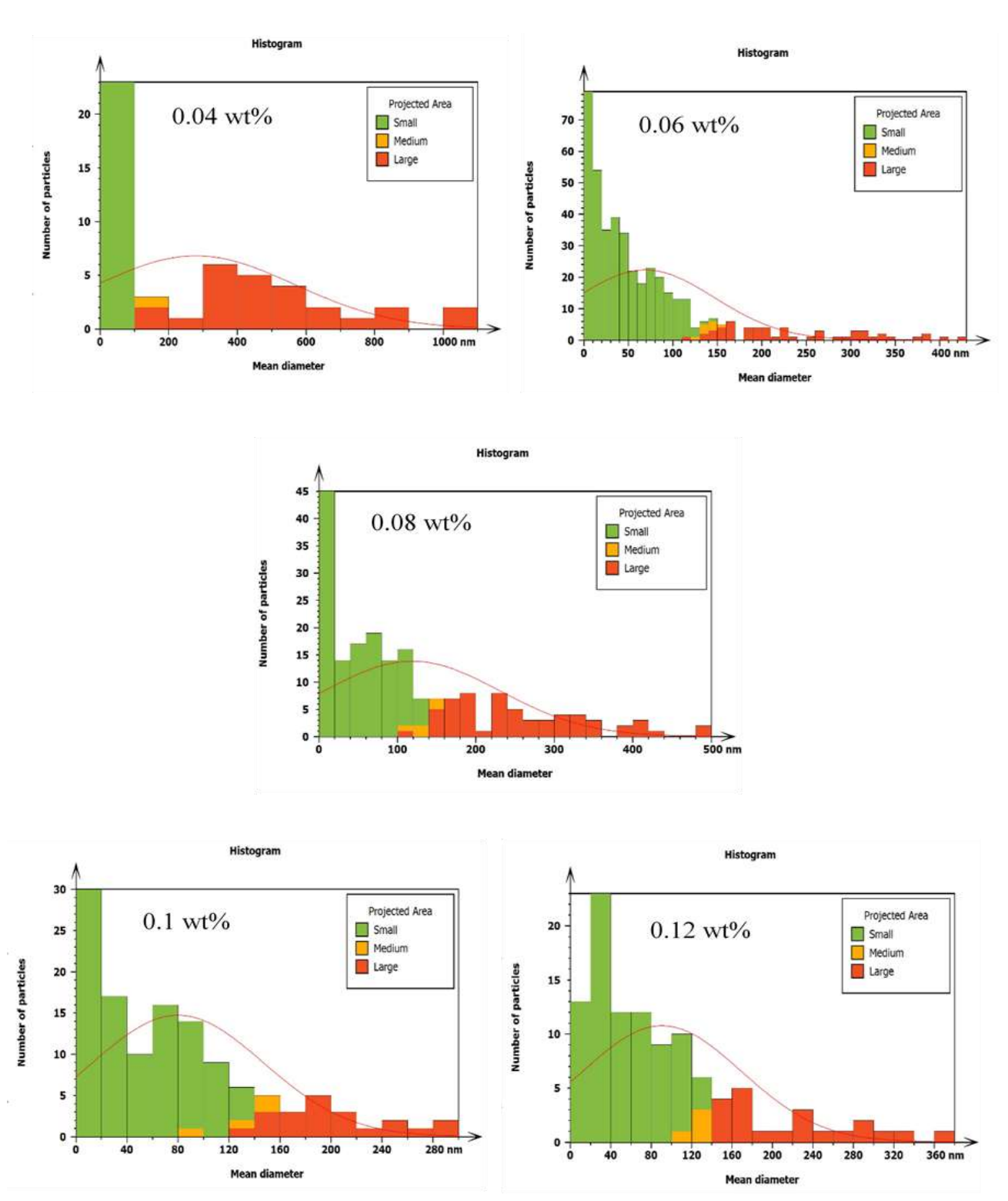
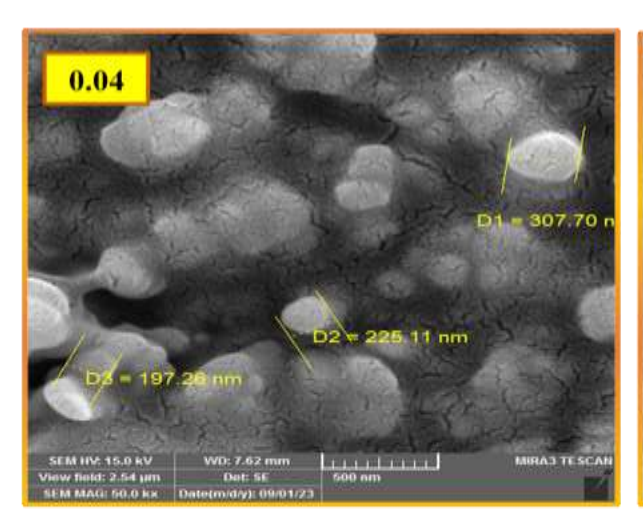
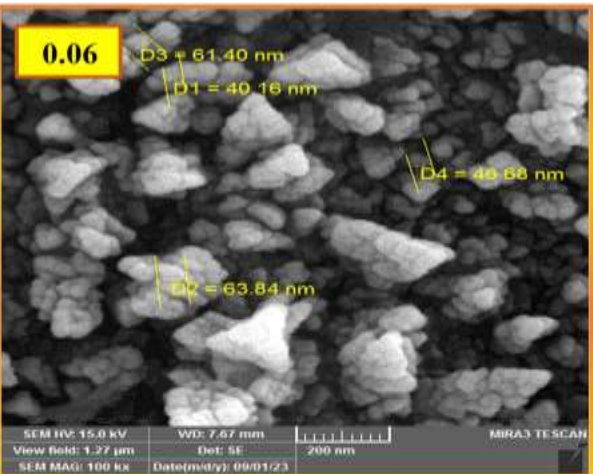
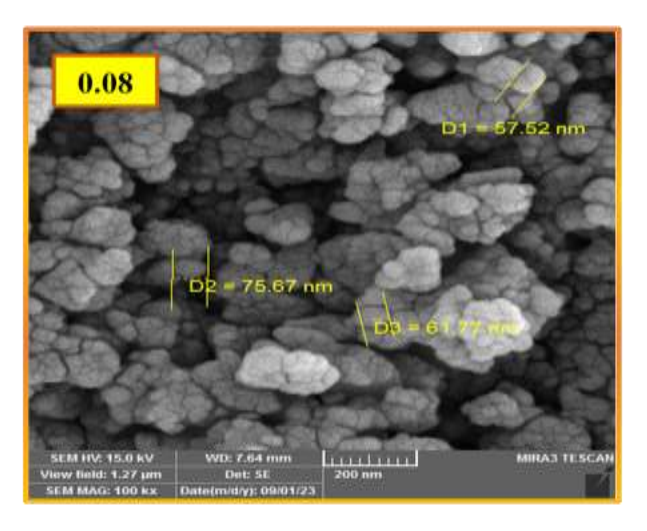


Figure 5: Granularity accumulation distribution charts for CBTS thin films at different thiourea concentrations.









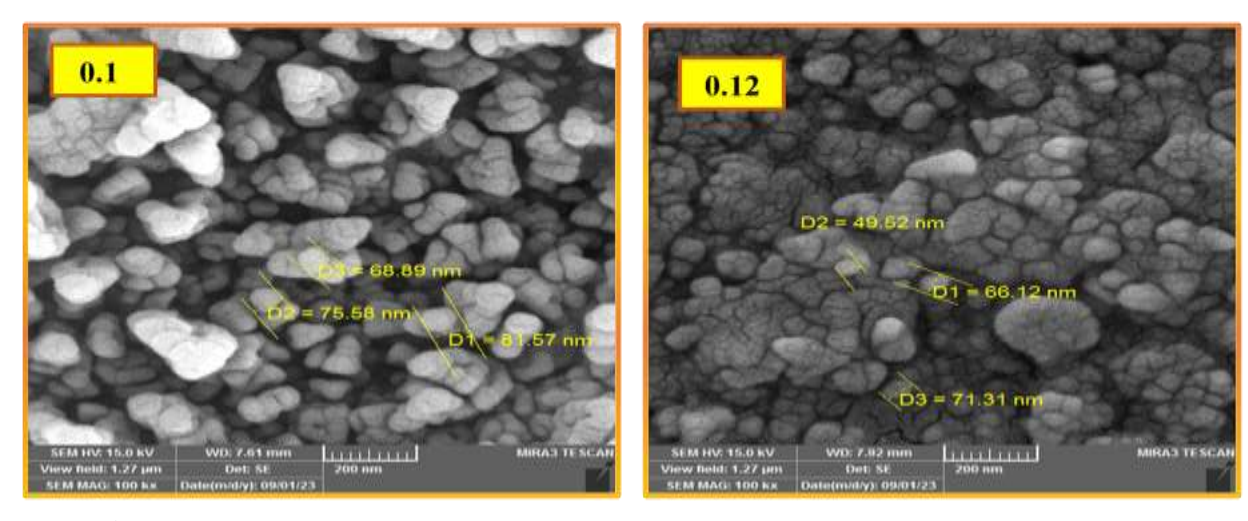


Figure 6: FE-SEM images for CBTS thin films at different thiourea concentrations.



Optical properties

Figure (7) illustrates the absorption spectra at (300-900) nm wavelengths of thin films at various concentrations of thiourea. It shows that the absorbance of all samples prepared decreases as the wavelength increases. This is due to the fact that photons with a higher energy can only interact with the material and generate electron-hole pairs that contribute to the conduction process. The deposition method, deposition parameters, and components of the substance all contribute to the spectral description of absorption. The degree of crystallization is a factor in the absorbance, it may not be accurate for every sample. This is due to the presence of localized states near the valence and conduction bands [27].

It is probable that grains and grain boundaries possess distinct characteristics, which serve as dispersal sources. The density of grain boundaries is subject to variation between samples depending on the particle size. Additionally, Contaminants near grain borders cause additional light dispersion, often worsening the disparity between the grains and the boundaries. Consequently, the transparency of the material is significantly influenced by the properties of particle boundaries [28].

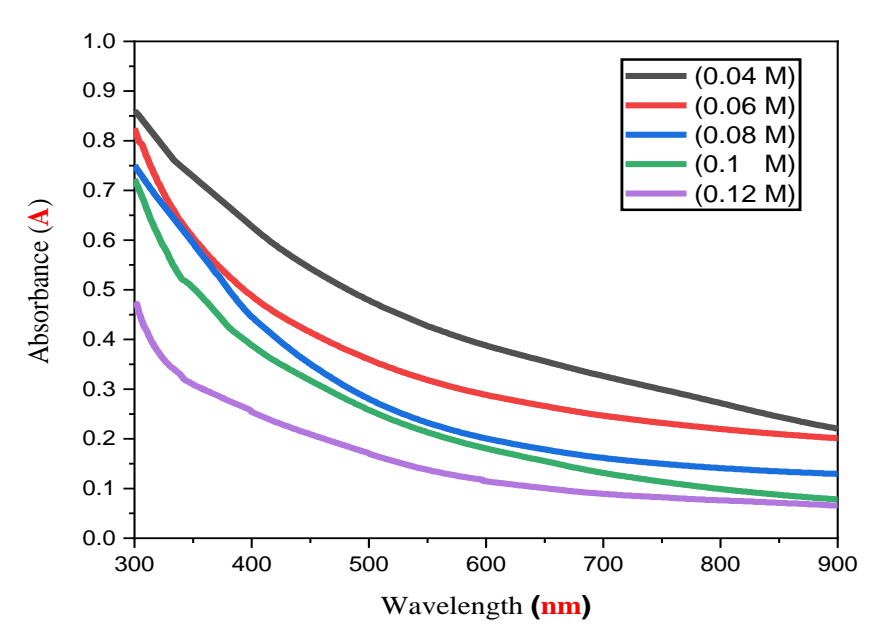


Figure 7: The absorbance for CBTS thin films at different thiourea concentrations. The absorption coefficient of thin films is calculated by using from the following equation:



$$\alpha = 2.303 \, \frac{A}{t} \tag{5}$$

Where A is the absorbance and t is the film's thickness. The absorption coefficient is a function of the incident photon energy for all prepared thin films, as illustrated in Figure (8). The absorption coefficient values of all thin films ($\geq 10^4$ cm⁻¹) are high at high energies [23,24], indicating the occurrence of allowed direct electronic transitions. The absorption coefficient exhibits a gradual evolution at low energies, which is subsequent to a rapid rise in values near the fundamental absorption energy [27].

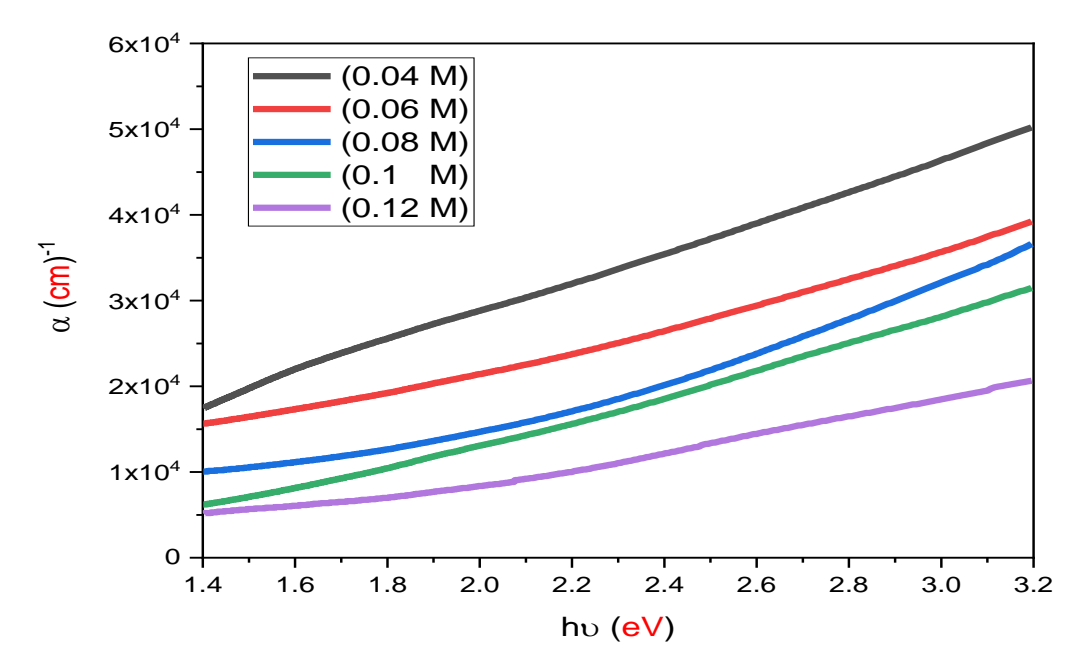


Figure 8: The absorption coefficient for CBTS thin films at different thiourea concentrations.

The energy gap of thin films can be calculated from the following:

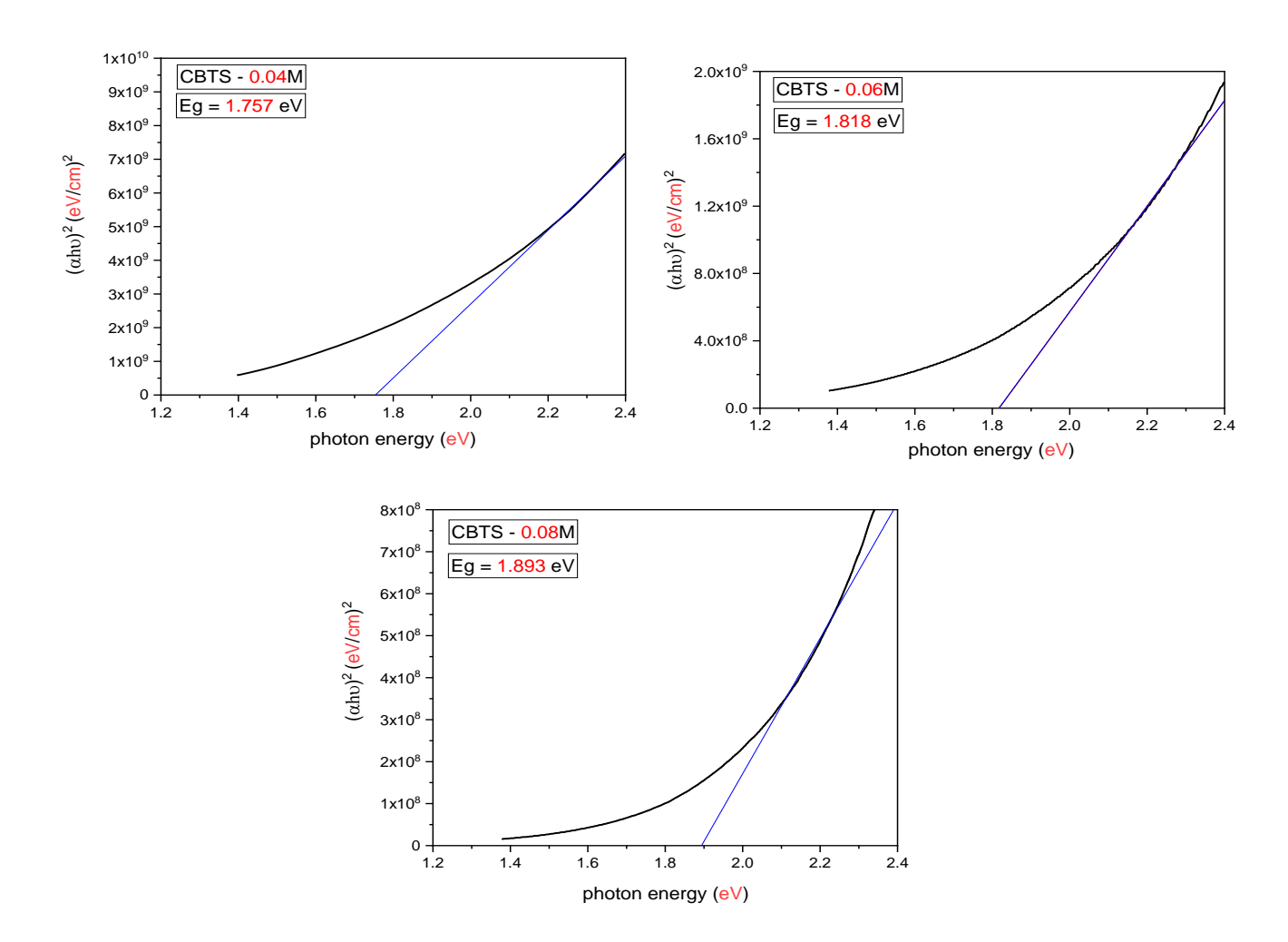
$$\alpha h v = B (h v - E_g)^n \tag{6}$$

The absorption coefficient α , incoming photon energy hu, energy bandgap E_g , constant B, and allowable direct transition with n = 1/2 are all defined in the equation.

The Tauc plot is a useful tool for estimating the energy gap of direct transition materials that are allowed. A linear relationship may be shown by graphing the square of (αhv) and (hv) in electron volts (eV). The determination of the material's direct band gap involves projecting this line to $(\alpha hv)^2 = 0$ [29].



This is illustrated in the Figure (9). The allowed direct band gap values range from (1.757 eV) for concentration (0.04 M) to (1.923 eV) for concentration) 0.12 M), with the values listed in Table (5) [30,31]. It can be observed that the energy gap values of the prepared thin films increase with increasing concentration of thiourea. We can figure out that there is a quantum size effect because the band gap energy is related to the size of the crystallites. This effect is similar to the quantum confinement effect and is controlled by the temperature of deposition [32].





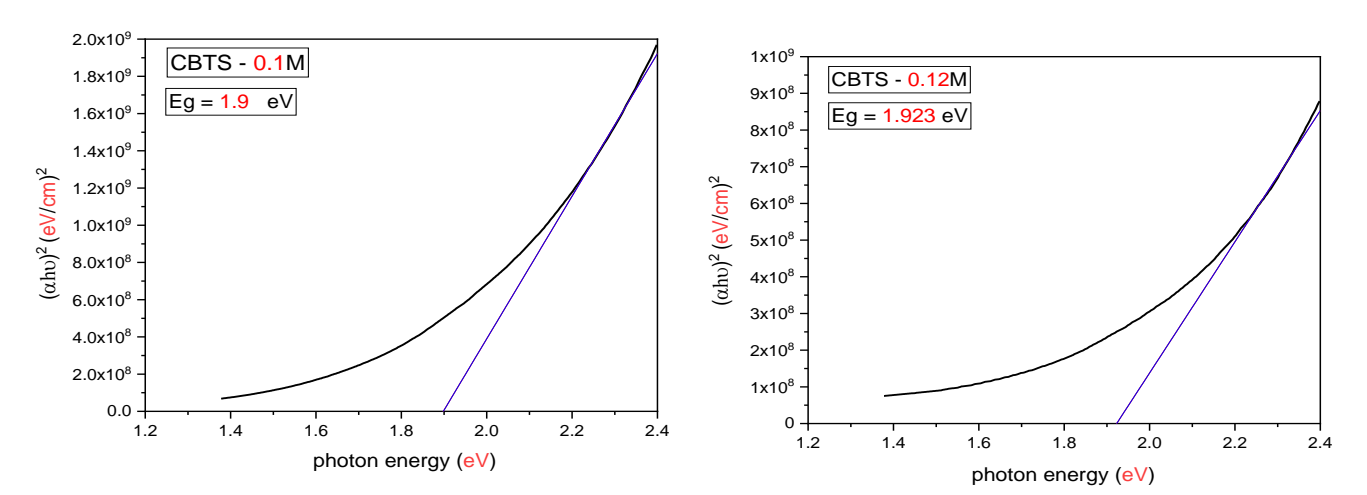


Figure 9: Optical energy gap for CBTS thin films at different thiourea concentrations.

Table 5: Optical energy gap for CBTS thin films at different thiourea concentrations.

Thiourea Concentration (M)	Energy band gap (eV)
0.04	1.757
0.06	1.818
0.08	1.893
0.1	1.9
0.12	1.923

Electrical properties

To study the electrical properties, the Hall Effect was investigated at room temperature for CBTS thin films at different concentrations of thiourea. The type, concentration, and mobility of majority charge carriers were determined. The results of the Hall Effect measurements are shown in Table (6). It is inferred that all thin films are p-type [33,34] according to the following equation:

$$\mathbf{R}_{\mathbf{H}} = \frac{\mathbf{E}_{\mathbf{y}}}{\mathbf{j}_{\mathbf{x}} \mathbf{B}_{\mathbf{z}}} = \frac{\mathbf{V}_{\mathbf{H}} \mathbf{t}}{\mathbf{I} \, \mathbf{B}} = \frac{1}{n_{\mathbf{H}}} \tag{7}$$

With positive Hall coefficient indicates that the majority of charge carriers are holes, while minority carriers are electrons [17]. Figure (10) shows (a. The Hall conductivity, b. Hall mobility, and c. Charge carriers) for CBTS thin films at different concentrations of thiourea. The Hall conductivity, Hall mobility and charge carriers increase with increasing thiourea concentration, while decreasing at higher thiourea concentrations. This result is associated with the growth of crystallites and particles in the formed thin films.



Table 6: Hall Effect measurement results for CBTS thin films at different thiourea concentrations.

Thiourea	R _H (cm ³ /C)	n×10 ¹⁶	μ	ρ	σ
concentration (M)		(cm ⁻³)	$(cm^2/(V.s))$	$(\Omega.cm)$	$(\Omega^{-1} \text{cm}^{-1})$
0.04	114.572	5.448	6.152	18.6235	0.053
0.06	83.999	7.430	8.114	10.3523	0.096
0.08	82.812	7.537	10.595	7.8161	0.127
0.1	69.290	9.008	12.761	5.4298	0.184
0.12	69.385	8.995	11.328	6.1251	0.163

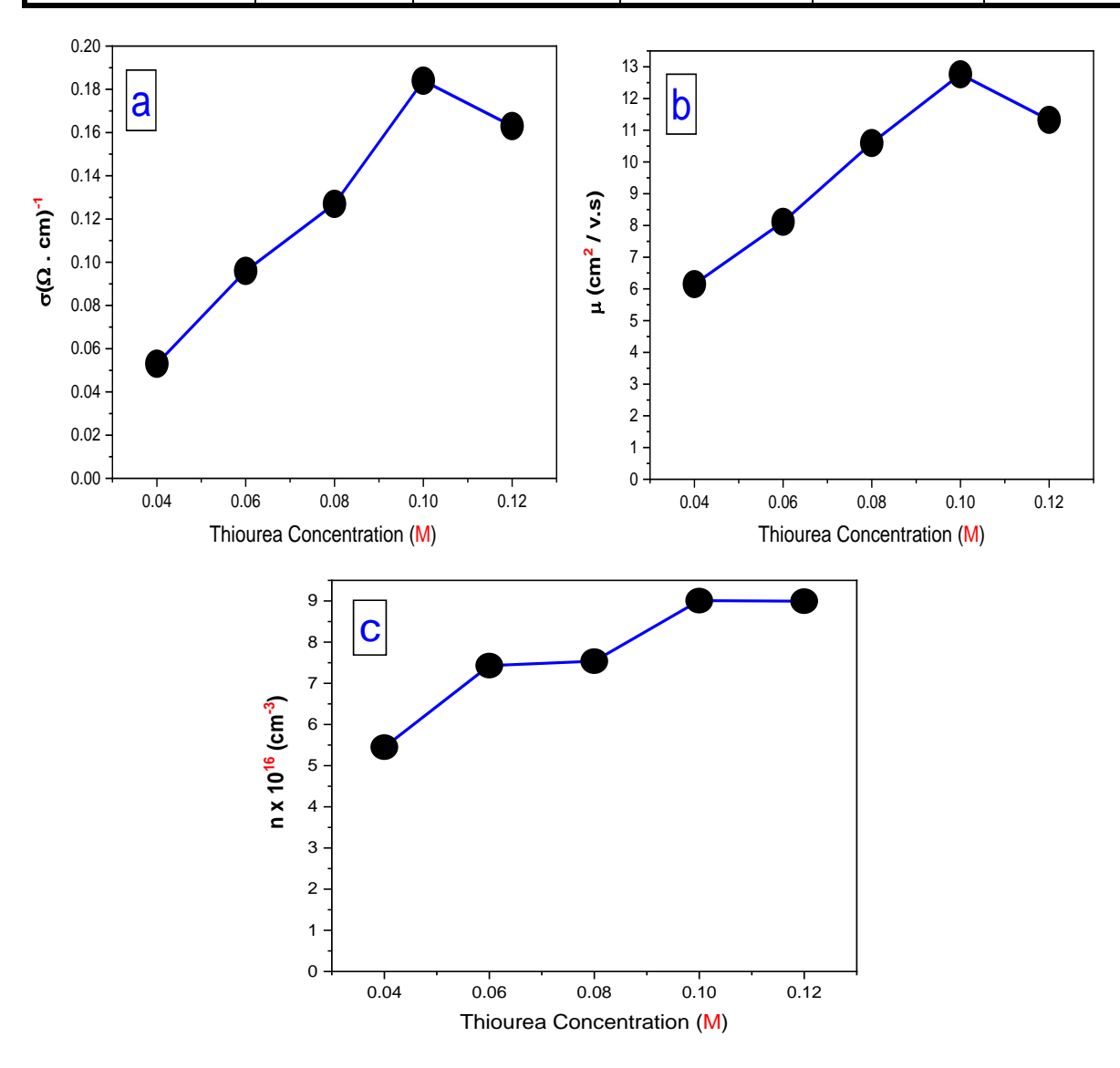


Figure 10: (a) The conductivity, (b) The mobility, (c) Charge carriers, for CBTS thin films at different thiourea concentrations.



The Hall Effect measurements indicated that the charge carriers are of the p-type. The maximum value for the conductivity and the mobility found in a thin film with concentration (0.01) M thiourea.

Conclusions

The CBTS thin films were effectively developed using the CSP method in this study. The spectra display a distinct broad and wide peak at approximately (341 cm $^{-1}$), which corresponds to trigonal CBTS. The FE-SEM images revealed a discrepancy in the surface of the films, which were dense and abrasive, and contained cavities and apertures with cauliflower-like structures. The optical tests revealed that the absorption coefficient values for all thin films at varying concentrations of thiourea ($\alpha \ge 10^4$ cm $^{-1}$) and the allowed direct band gap values range from (1.757 to 1.923) eV and Hall mobility values range from (6.152 to 12.761) cm 2 V $^{-1}$ S $^{-1}$ and p-type conductivity have been determined to be suitable for solar cell applications.

Source of funding: Source of funding: This research received no funding from any agency.

Conflict of interest: The authors declare that there is no conflict of interest.

Ethical clearance: Ethical approval was not required for this study.

References

- [1] S. Nivetha, K. Kaviyarasu, A. Ayeshamariam, N. Punithavelan, R. Perumalsamy, A. K. Diallo, G. Ramalingam, S. B. Mohamed, D. Letsholathebe, C. M. Magdalane, M. Jayachandran, Optical and Structural Properties of Fluorine Doped SnO₂ on Si (100) for Photovoltaic Application, Journal of Nanoelectronics and Optoelectronics, (2018), DOI(https://doi.org/10.1166/jno.2018.2383)
- [2] Y. Thaver, S.O. Oseni, & G.T. Mola, Silver doped nickel oxide nanocomposite and photon harvesting enhancement in bulk heterojunction organic solar cell, Solar Energy, 214, 11-18 (2021), DOI(https://doi.org/10.1016/j.solener.2020.11.044)
- [3] S. Sebastian, I. Kulandaisamy, S. Valanarasu, I.S. Yahia, H. Kim, & D. Vikraman, Microstructural and electrical properties evaluation of lead doped tin sulfide thin films, Journal of Sol-Gel Science and Technology, 93, 52-61(2019), DOI(https://doi.org/10.1007/s10971-019-05169-y)



- [4] A.C. Lokhande, K.V. Gurav, E.A. Jo, C.D. Lokhande, & J.H. Kim, Chemical synthesis of Cu₂SnS₃ (CTS) nanoparticles: A status review, Journal of Alloys and Compounds, 656, 295-310(2016), DOI(https://doi.org/10.1016/j.jallcom.2015.09.232)
- [5] D. Naveena, T. Logu, R. Dhanabal, K. Sethuraman, & A.C. Bose, Comparative study of effective photoabsorber CuO thin films prepared via different precursors using chemical spray pyrolysis for solar cell application, Journal of Materials Science: Materials in Electronics, 30, 561-572(2019), DOI(https://doi.org/10.1007/s10854-018-0322-4)
- [6] M. N. Harif, K.S. Rahman, C. Doroody, H.N. Rosly, M. Isah, M.A. Alghoul, H. Misran, & N. Amin, Microstructural evolution of oxygen incorporated CdTe thin films deposited by close-spaced sublimation, Materials Letters, (2021), DOI(https://doi.org/10.1016/j.matlet.2021.130552)
- [7] A. Kotbi, B. Hartiti, S. Fadili, A. Ridah, & P. Thevenin, Some physical parameters of CuInGaS₂ thin films deposited by spray pyrolysis for solar cells, Applied Physics A, 123, 1-8 (2017), DOI(https://doi.org/10.1007/s00339-017-0981-7)
- [8] A. Ziti, B. Hartiti, H. Labrim, S. Fadili, A. Batan, M. Tahri, A. Ridah, O. Mounkachi, A. Benyoussef, & P. Thevenin, Characteristics of kesterite CZTS thin films deposited by dip-coating technique for solar cells applications, Journal of Materials Science: Materials in Electronics, 1-10(2019), DOI(https://doi.org/10.1088/1402-4896/ac6d1f)
- [9] M. A. Green, E.D. Dunlop, J. Hohl-Ebinger, M. Yoshita, N. Kopidakis, & X. Hao, Progress in Photovoltaics: Research and Applications, 29, 15 – 3(2020), DOI(<u>https://doi.org/10.1002/pip.3303</u>)
- [10] C. Malerba, F. Biccari, C.L. Azanza Ricardo, M. Valentini, R. Chierchia, M. Müller, A. Santoni, E.M. Esposito, P. Mangiapane, P. Scardi, & A. Mittiga, CZTS stoichiometry effects on the band gap energy, Journal of Alloys and Compounds, 582, 528-534(2014), DOI(https://doi.org/10.1039/C6TA01558A)
- [11] S. M. Abdullah, N.A. Bakr, & S.A. Salman, Structural, optical, and electrical properties of Ag₂ZnSnS₄ sprayed thin films by chemical pyrolysis method, Chalcogenide Letters, (2021), DOI(https://doi.org/10.15251/CL.2021.182.65)



- [12] I. M. El Radaf, & H.Y. Al-Zahrani, Facile Synthesis and Structural, Linear and Nonlinear Optical Investigation of p-type Cu₂ZnGeS₄ Thin Films as a Potential Absorber Layer for Solar Cells, Journal of Electronic Materials, 49, 4843 – 4851(2020), DOI(https://doi.org/10.1016/j.tsf.2019.02.049)
- [13] I. M. El Radaf, H. I. Elsaeedy, H. A. Yakout, & M. T. El Sayed, Junction Parameters and Electrical Characterization of the Al/n-Si/Cu₂CoSnS₄/Au Heterojunction, Journal of Electronic Materials, 48, 6480 6486(2019), DOI(https://doi.org/10.1007/s11664-019-07445-7)
- [14] S. Dridi, N. Bitri, & M. Abaab, Synthesis of quaternary Cu₂NiSnS₄ thin films as a solar energy material prepared through «spray» technique, Materials Letters, 204, 61-64(2017), DOI(https://doi.org/10.1016/j.matlet.2017.06.028)
- [15] X. Miao, R. Chen, & W. Cheng, Synthesis and characterization of Cu₂FeSnS₄ thin films prepared by electrochemical deposition, Materials Letters, 193, 183-186(2017), DOI(https://doi.org/10.1016/j.matlet.2017.01.099)
- [16] Y. Al-Douri, A. O. Odeh, M.R. Johan, Z. Z. Chowdhury, R. F. Rafique, A. H. Reshak, & C. H. Voon, Synthesis and Characterization of Cu₂CdSnS₄ Quaternary Alloy Nanostructures, International Journal of Electrochemical Science, (2018), DOI(https://doi.org/10.20964/2018.07.45)
- [17] H. Guo, C. Ma, Z. Chen, X. Jia, Q. Cang, N. Yuan, & J. Ding, The fabrication of Cu₂BaSnS₄ thin film solar cells utilizing a maskant layer, Solar Energy, (2019), DOI(https://doi.org/10.1016/j.solener.2019.02.007)
- [18] Z. Chen, K. Sun, Z. Su, F. Liu, D. Tang, H. Xiao, L. Shi, L. Jiang, X. Hao, & Y. Lai, Solution-Processed Trigonal Cu₂BaSnS₄ Thin-Film Solar Cells, ACS Applied Energy Materials, (2018), DOI(https://doi.org/10.1021/acsaem.8b00514)
- [19] M. S. Kumar, S. P. Madhusudanan, S. C. Kanth, K. Mohanta, & S. K. Batabyal, Solution phase fabrication of photoactive Cu₂BaSnS₄ thin films for solar energy harvesting, Journal of solid state electrochemistry, 24, 305-311(2019), DOI(https://doi.org/10.1007/s10008-019-04418-y)



- [20] M. S. Kumar, S. P. Madhusudanan, & S. K. Batabyal, Solution-processed photoactive trigonal Cu₂BaSnS₄ thin films for efficient solar energy harvesting, Materials Characterization, 174, 110988(2021), DOI(https://doi.org/10.1016/j.matchar.2021.110988)
- [21] E. Djatoubai, & J. Su, First spray pyrolysis thin film fabrication of environment-friendly Cu₂BaSnS₄ (CBTS) nanomaterials. Chemical Physics Letters, 770, 138406(2021), DOI(https://doi.org/10.1016/j.cplett.2021.138406)
- [22] J. Leng, Z. Wang, J. Wang, H. Wu, G. Yan, X. Li, H. Guo, Y. Liu, Q. Zhang, & Z. Guo, Advances in nanostructures fabricated via spray pyrolysis and their applications in energy storage and conversion, Chemical Society reviews, 48 11, 3015-3072(2019), DOI(https://doi.org/10.1039/C8CS00904J)
- [23] H. Luo, J. Chen, X. Zhang, S. Wang, H. Gu, W. Wang, & H. Li, Controlled synthesis of high efficiency Cu₂BaSnS₄ solar cells via a solution processed method, Materials Letters, 270, 127750(2020), DOI(https://doi.org/10.1016/j.matlet.2020.127750)
- [24] A. Ziti, B. Hartiti, S, Smairi, H. Labrim, Y. Nouri, H.J. Nkuissi, & P. Thevenin, Optical investigations of Cu₂BaSnS₄ quaternary nanostructure absorbers deposited by dip-coating technique, Journal of Materials Science: Materials in Electronics, 33(32), 24477-24492(2022), DOI(https://doi.org/10.1007/s10854-022-09160-2)
- [25] X. Zhang, E. Fu, Y. Wang, & C. Zhang, Fabrication of Cu₂ZnSnS₄ (CZTS) nanoparticle inks for growth of CZTS films for solar cells, Nanomaterials, 9(3), 336(2019), DOI(https://doi.org/10.3390/nano9030336)
- [26] P. S. Maldar, A. Mane, S. S. Nikam, S. D. Dhas, & A. V. Moholkar, Spray deposited Cu₂CoSnS₄ thin films for photovoltaic application: Effect of film thickness, Thin Solid Films, 709, 138236(2020), DOI(https://doi.org/10.1016/j.tsf.2020.138236)
- [27] A. D. Sharma, P. Sahoo, A. K. Singha, S. Padhan, & R. Thangavel, Visible-light induced photosplitting of water using solution-processed Cu₂BaSnS₄ photoelectrodes and a tandem approach for development of Pt-free photoelectrochemical cell, Materials Science in Semiconductor Processing, 121, 105433(2021), DOI(https://doi.org/10.1016/j.mssp.2020.105433)



- [28] W. D. Callister Jr, & D. G. Rethwisch, Fundamentals of Materials Science and Engineering: n Integrated Approach, 5th Edition. (John Wiley & Sons, New Jersey, 2018), 817-821
- [29] J. Robertson, Electronic structure of amorphous semiconductors, Advances in Physics, 32(3), 361–452(1983), DOI(https://doi.org/10.1080/00018738300101571)
- [30] F. Hong, W. Lin, W. Meng, & Y. Yan, Trigonal Cu₂-II-Sn-VI₄ (II= Ba, Sr and VI= S, Se) quaternary compounds for earth-abundant photovoltaics, Physical Chemistry Chemical Physics, 18(6), 4828-4834(2016), DOI(https://doi.org/10.1039/C5CP06977G)
- [31] J. Ge, P. Koirala, C. R. Grice, P. J. Roland, Y. Yu, X. Tan, R. J. Ellingson, R. W. Collins, & Y. Yan, Oxygenated CdS Buffer Layers Enabling High Open–Circuit Voltages in Earth–Abundant Cu₂BaSnS₄ Thin–Film Solar Cells, Advanced Energy Materials, 7(6), 1601803, (2017), DOI(https://doi.org/10.1002/aenm.201601803)
- [32] S. J. Ikhmayies, & R. N. Ahmad-Bitar, A study of the optical bandgap energy and Urbach tail of spray-deposited CdS: In thin films, Journal of Materials Research and Technology, 2(3), 221-227(2013), DOI(https://doi.org/10.1016/j.jmrt.2013.02.012)
- [33] N. Mahdi, & N.A. Bakr, Effect of Na Doping on Some Physical Properties of Chemically Sprayed CZTS Thin Films, East European journal of physics, 3, 84-90(2022), DOI(https://doi.org/10.26565/2312-4334-2022-3-11)
- [34] R. A. Abdullah, N. A. Bakr, & K. Diwate, Physical properties of Cu₂MgSnS₄ thin films prepared by chemical spray pyrolysis technique: The effect of thiourea concentration, Chalcogenide Letters, (2022), DOI(https://doi.org/10.15251/CL.2022.1910.691)